Structure, Vol. 13, 1725–1735, November, 2005, ©2005 Elsevier Ltd All rights reserved. DOI 10.1016/j.str.2005.09.006

A Structure of the Human Apoptosome at 12.8 Å Resolution Provides Insights into This Cell Death Platform

Xinchao Yu,[1] Devrim Acehan,[1] Jean-François Ménétret,[1] Christopher R. Booth,[3] Steven J. Ludtke,[3] Stefan J. Riedl,[4] Yigong Shi,[4] Xiaodong Wang,[2] and Christopher W. Akey[1,*]

[1]Department of Physiology and Biophysics
Boston University School of Medicine
700 Albany Street
Boston, Massachusetts 02118

[2]Howard Hughes Medical Institute and Department of Biochemistry
University of Texas Southwestern Medical Center at Dallas
Dallas, Texas 75235

[3]National Center for Macromolecular Imaging
Verna and Marrs McLean Department of Biochemistry and Molecular Biology
Baylor College of Medicine
1 Baylor Plaza
Houston, Texas 77030

[4]Department of Molecular Biology
Princeton University
Lewis Thomas Laboratory
Princeton, New Jersey 08544

Summary

Apaf-1 and cytochrome c coassemble in the presence of dATP to form the apoptosome. We have determined a structure of the apoptosome at 12.8 Å resolution by using electron cryomicroscopy and single-particle methods. We then docked appropriate crystal structures into the map to create an accurate domain model. Thus, we found that seven caspase recruitment domains (CARDs) form a central ring within the apoptosome. At a larger radius, seven copies of the nucleotide binding and oligomerization domain (NOD) associate laterally to form the hub, which encircles the CARD ring. Finally, an arm-like helical domain (HD2) links each NOD to a pair of β propellers, which bind a single cytochrome c. This model provides insights into the roles of dATP and cytochrome c in assembly. Our structure also reveals how a CARD ring and the central hub combine to create a platform for procaspase-9 activation.

Introduction

Programmed cell death terminates cells in an orderly fashion to benefit the organism (Desagher and Martinou, 2000). Caspases are the executioners of this pathway and use an essential cysteine to cleave target proteins after aspartate residues (Song and Steller, 1999). In apoptosis, death signals activate initiator caspases, which then cleave downstream zymogens to create active executioner caspases. This process leads to the hallmarks of apoptosis that include chromatin degradation and organelle destruction (Budihardjo et al., 1999; Salvesen and Dixit, 1997). Apoptosis plays a decisive role in sculpting the embryo and in maintaining tissue homeostasis in adults (Ferraro et al., 2003). In addition, the transition to unrestrained cell growth in some cancers may require the activation of oncogenes and the downregulation of apoptotic pathways (Song and Steller, 1999; Salvesen and Dixit, 1997). Thus, apoptotic pathways provide a brake against certain cancers and autoimmunity diseases (Green and Evan, 2002). Conversely, apoptosis may be upregulated in AIDS, neurodegenerative diseases, and ischemic stroke (Thompson, 1995; Danial and Korsmeyer, 2004).

The intrinsic cell death pathway recognizes developmental cues, genomic stress, or cytotoxic damage (Wang, 2001; Newmeyer and Ferguson-Miller, 2003). In this pathway, the Bcl family acts as a master switching system that integrates pro-life and death signals (Kuwana and Newmeyer, 2003; Desagher and Martinou, 2000). Activation of pro-death Bcl family members leads to the release of proapoptotic factors from mitochondria that include cytochrome c, Smac/DIABLO, EndoG, AIF, and HtrA2/Omi (see Green and Evan, 2002; Wang, 2001). In particular, cytochrome c undergoes a rapid release from mitochondria (Goldstein et al., 2000) and plays a critical role in Apaf-1 oligomerization, which leads to procaspase-9 activation (Hu et al., 1999; Srinivasula et al., 1998; Li et al., 1997; Liu et al., 1996).

Apaf-1 is the cardinal member of a family of large P loop NTPases that have multiple domains (Zou et al., 1997; Leipe et al., 2004; Inohara and Nunez, 2003). Apaf-1 contains an N-terminal caspase recruitment domain (CARD), a nucleotide binding and oligomerization domain (NOD), and a C-terminal regulatory region comprised of 13 WD40 repeats that form two β propellers (Acehan et al., 2002; Hu et al., 1998; Zou et al., 1999). Apaf-1 exists in an inactive, latent state in cells, and single-particle images suggest that the Y-shaped monomer may adopt a compact structure (Acehan et al., 2002). The latent state probably results from the self-chaperoning activity of two β propeller domains, as Apaf-1 molecules without this regulatory region were found to be constitutively active in the absence of cytochrome c (Hu et al., 1999; Srinivasula et al., 1998). Hence, Apaf-1 may undergo a significant conformational change upon binding cytochrome c and dATP/ATP, which triggers apoptosome assembly (Acehan et al., 2002; Jiang and Wang, 2000). The apoptosome then binds procaspase-9 (Rodriguez and Lazebnik, 1999; Zou et al., 1999; Hu et al., 1999), and interdomain cleavage of the zymogen is not required for activation (Stennicke et al., 1999; Srinivasula et al., 1998; Acehan et al., 2002). Remarkably, the apoptosome/procaspase-9 complex forms a holo-enzyme whose ability to cleave caspase-3 is ~2000 times higher than for released caspase-9 (Chao et al., 2005; Stennicke et al., 1999; Rodriguez and Lazebnik, 1999). The mechanism of procaspase-9 activation is controversial and may involve dimerization of monomeric procaspase-9 on the apoptosome (Boatright et al., 2003; Acehan et al., 2002; Renatus et al., 2001), or

*Correspondence: cakey@bu.edu

it may require conformational changes of the zymogen induced by its association with this platform (Chao et al., 2005; Shi, 2002).

The apoptosome can be assembled from recombinant Apaf-1 and cytochrome c (Hu et al., 1999; Srinivasula et al., 1998; Li et al., 1997; Liu et al., 1996), and structural electron microscopy (EM) of this complex revealed a wheel-like particle with seven subunits and a mass of ~1 MDa (Acehan et al., 2002). The first map at ~27 Å resolution allowed a tentative identification of CARD, NOD, and WD40 domains within the apoptosome and suggested that cytochrome c may be bound between two β propellers in the regulatory region. A recent crystal structure of Apaf-1 without its regulatory WD40 motifs (Apaf1-591) has now revealed the atomic structure of three distinct domains within the NOD and a fourth superhelical domain (HD2; Riedl et al., 2005). In this structure, domains of the NOD form an enclosed binding pocket for ADP. However, the relationship between the Apaf1-591 crystal structure and its conformation within the apoptosome remains unknown.

In this paper, we present a significantly improved structure of the human apoptosome at ~12.8 Å resolution. We then used crystal structures to model the domain architecture of the human apoptosome. This analysis provides direct insights into apoptosome assembly and into the roles of a CARD ring and the NOD in procaspase-9 activation.

Results

Apoptosome Stability and Structure Determination

The active isoform of Apaf-1 contains 13 WD40 repeats in the regulatory region (see Zou et al., 1999; Hu et al., 1999; Srinivasula et al., 1998). We overexpressed this isoform in insect cells and used the purified Apaf-1 to assemble apoptosomes in buffer A with cytochrome c and dATP. These apoptosomes migrated on a glycerol gradient as large complexes and contain cytochrome c (Figure 1A, left; standard assembly). However, previous immunoprecipitation experiments suggested that cytochrome c may dissociate from apoptosomes in cell lysates after Apaf-1 assembly (Hill et al., 2004). Thus, we asked whether cytochrome c is a subunit of the apoptosome under near physiological conditions. To answer this question, we assembled apoptosomes in buffer A supplemented with KCl to a final concentration of 100 mM and ran the complexes on a glycerol gradient in this buffer. Under these conditions, we found that cytochrome c remains bound to the apoptosome (Figure 1A, middle; 100 mM KCl). We conclude that cytochrome c forms a stable interaction with the apoptosome in physiological salt at pH 7.5.

Previous studies at 27 Å resolution showed that the apoptosome has a wheel-like architecture with seven spokes radiating from a central hub (Acehan et al., 2002; Figure S1, left; see the Supplemental Data available with this article online). To obtain an improved 3D map, we collected a data set of ~10,000 particles from specimens frozen in buffer over holes with an acceleration voltage of 200 kV for the electron beam. We processed the particles in EMAN (Ludtke et al., 1999) and obtained a 3D structure with a resolution of ~21 Å from ~5,400 particles (Figure S1, middle). This map confirmed the general architecture of the apoptosome and revealed additional features that had not been observed previously. However, the resolution of this map appeared to be limited by several factors. First, the apoptosome is ~270 Å in diameter with a maximal thickness of ~70 Å. Thus, its geometry may be conducive to an intrinsic flexibility of the Y-shaped regulatory regions. Second, this geometry also produces low contrast for top or oblique views in frozen buffer. This problem was especially acute in micrographs taken close to focus, which record higher-resolution information. To improve contrast, we collected a second data set of ~13,000 apoptosomes in which the ice thickness was just sufficient to allow different particle orientations, and we used a lower acceleration voltage (120 kV).

A histogram of the predicted resolution for each particle from the final data set is shown in Figure S2. After the data were processed in EMAN (Ludtke et al., 2004), a final 3D map was obtained from ~7,600 particles with a resolution of ~12.8 Å ($FSC_{0.5}$, Figure 1B). A top view of the final 3D map is shown in Figure 1C and reveals a greater wealth of detail than seen previously. This is particularly evident in surface views related by rotations about the horizontal axis (Figure 1D). In the map, seven features have been resolved on the central hub that form a "crown," a central CARD ring is evident in the oblique bottom view, a small spur is resolved on the arm, and cytochrome c can be identified between two cylindrical β propellers in the regulatory region. We note that the absolute hand of the apoptosome was chosen arbitrarily in previous work (Acehan et al., 2002). However, our docking experiments have now revealed the absolute hand, which is inverted relative to that used previously (see Experimental Procedures). This handedness has been used in this paper.

Apaf-1 contains seven major domains and four linkers based on sequence homology and crystal structures (Riedl et al., 2005; Qin et al., 1999). In this report, we color coded these domains for clarity, as shown in Figure 2A. Starting at the N terminus, the CARD is followed by a short linker (L1), a nucleotide binding α/β domain (NBD) with Walker A and B boxes, a small helical domain (HD1), a second linker (L2), and a conserved, winged helix domain (WHD). A superhelical domain (HD2) extends to within ~10–20 residues of the first WD40 repeat, and a third linker (L3) may be present at this junction (Riedl et al., 2005). Finally, the WD40 repeats occur in groups of seven and six with a linker (L4) between them. Importantly, the WD40 repeats are known to form β propellers that regulate assembly (Acehan et al., 2002; Hu et al., 1999; Srinivasula et al., 1998).

To interpret the structure of the apoptosome, we docked "domain" crystal structures of Apaf1-591 (Figure 2B), cytochrome c, and β propellers from transducin Gβ (seven blades) and TolB (six blades) into the density map and then generated the 7-fold symmetry mates. We next used RsRef and manual adjustments in O (Jones et al., 1991) to refine the position of each domain (Fabiola and Chapman, 2005). This docking provided an accurate domain model of the apoptosome. However, we did not create a pseudoatomic model because the resolution of the map is too low and atomic structures are not available for the Apaf-1 β propellers. Even with these limitations, our model now gives a detailed

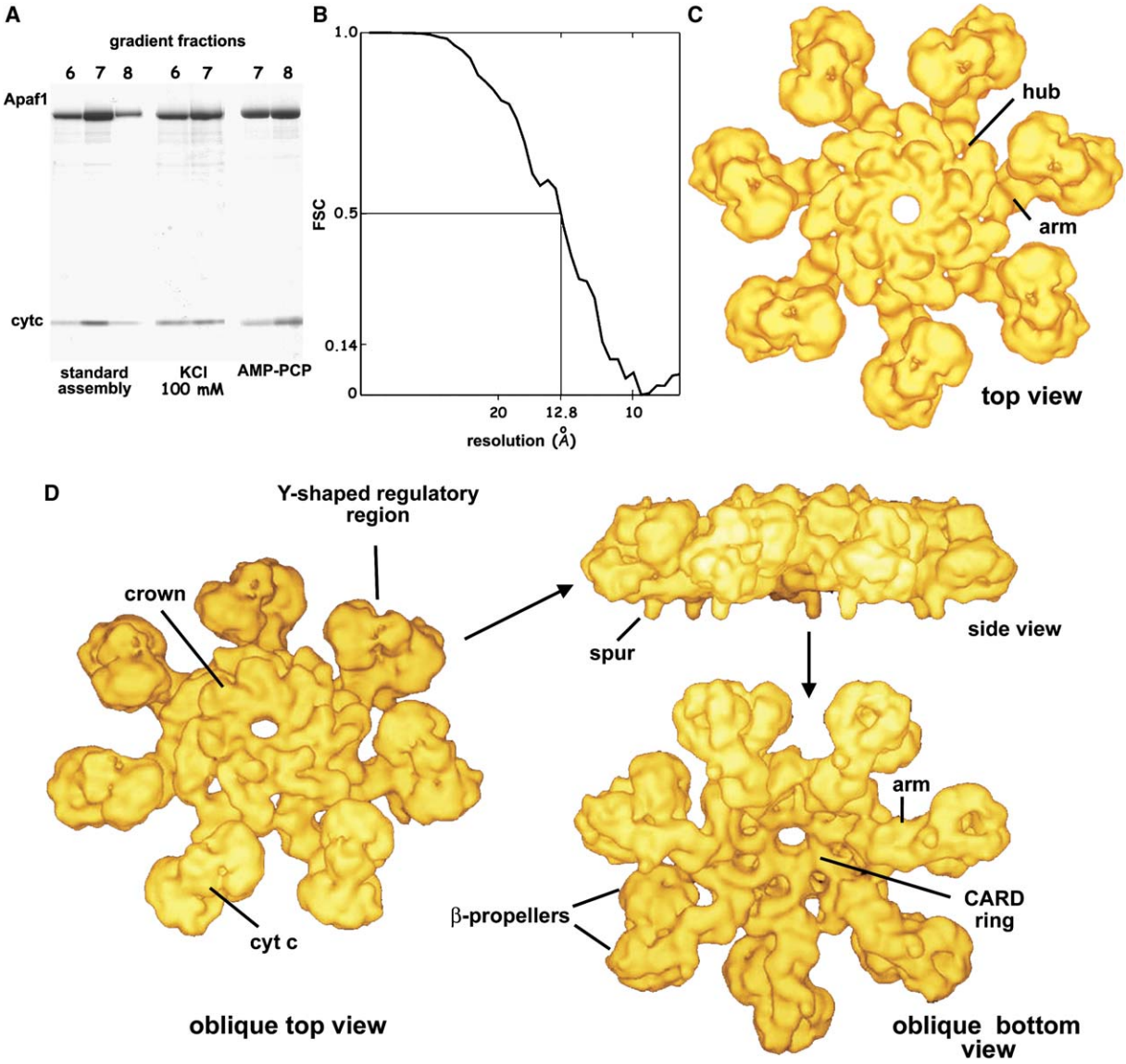

Figure 1. Stability and Structure of the Human Apoptosome

(A) (Left) The apoptosome runs in fractions 6–8 on a 10%–40% glycerol gradient after a standard assembly reaction. Under these conditions, GroEL (~800 kDa) ran in fraction 8 (not shown). (Middle) Cytochrome c remains bound to the apoptosome in 100 mM KCl. (Right) The recombinant apoptosome assembles in 0.1 mM AMP-PCP and $MgCl_2$ and retains cytochrome c during sedimentation.

(B) The resolution of the final 3D map (~12.8 Å) was determined from half-data sets by using the $FSC_{0.5}$ criterion.

(C) The apoptosome is viewed down the 7-fold axis. In this top view, features of the wheel-like particle, including the central hub and arms, are revealed.

(D) Three different views of the Apaf-1 apoptosome are shown as surfaces related by an in-plane rotation about the horizontal axis. Important regions are labeled and include: a central CARD ring, the crown, an arm, β propellers in the Y-shaped regulatory region, bound cytochrome c, and a spur-like feature.

snapshot of the apoptosome and provides direct insights into its assembly and function.

The CARD Ring

The N-terminal CARD represents the active site for procaspase-9 binding (Qin et al., 1999). We suggested previously that CARDs may occupy a central region within the apoptosome, based on docking experiments and the observation that procaspase-9 binds to the top surface of the hub (Acehan et al., 2002). In the new map, a central ring is clearly evident in a bottom view (Figure 2C). By a process of elimination, we accounted for all other Apaf-1 domains within the map (see next sections). The central ring remains and therefore must contain CARDs from seven Apaf-1 subunits. However, this region was the hardest to dock uniquely, because of the small size of the CARDs and due to a paucity of information on lateral CARD-CARD interactions. Nevertheless, we were able to choose an orientation such that seven CARDs fit within the map without major clashes, while placing the procaspase-9 binding site on the top surface (Figures 2D and 2E).

Our 3D map suggests that the CARDs form a discrete ring within the apoptosome, due to extensive lateral

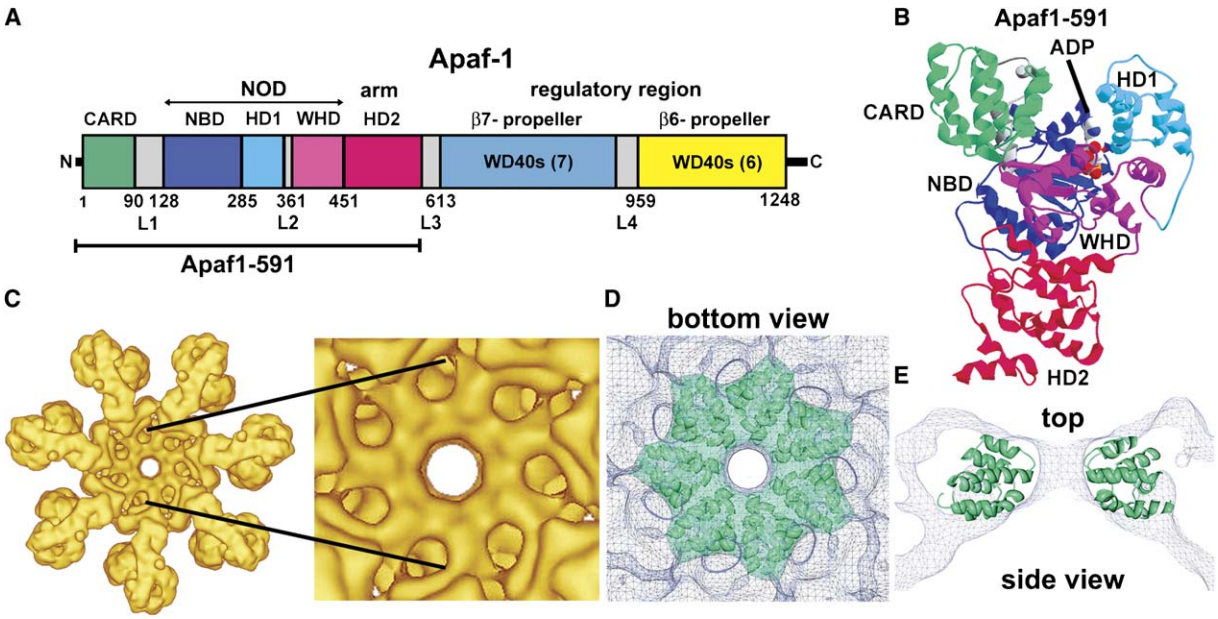

Figure 2. An Overview of Apaf-1 and Analysis of the CARD Ring

(A) A linear diagram of Apaf-1 is shown with color-coded domains. Linkers are shown in gray.
(B) Apaf1-591 is shown with color-coded ribbons. The ADP binding pocket is indicated near the top of the molecule.
(C) A ring at the center of the apoptosome (left) is visible in an expanded view of the bottom surface (right).
(D) Seven CARDs form a central ring within the apoptosome and are shown as green ribbons within a calculated molecular surface.
(E) Two oppositely facing CARDs within the central ring are shown in a thin density slab, as viewed from the side. The procaspase-9 binding surface is on the top surface of the CARD ring.

interactions that may involve the L1 linker. This link between the CARD and NBD (residues 100–120) is comprised of extended loops and two short α helices (Riedl et al., 2005) and is long enough to span the distance between a CARD and the NBD (~40 Å). However, we have not modeled the L1 linker because of its size. Hence, it is not clear which CARD represents the N-terminal domain of a particular monomer, because there are two possible choices within the CARD ring for each Apaf-1. Even so, we conclude that the CARD ring defines the active center of the apoptosome.

Architecture of the Central Hub and Arm

The nucleotide binding and oligomerization domain (NOD) forms part of the central hub (Acehan et al., 2002) and, thus, may play a critical role in forming the apoptosome. To evaluate this idea, Apaf-1 domains were docked within the central hub and arm of the apoptosome as follows. We started with HD2 because it has a short linker (~3 residues) that connects this domain to the winged helix domain. We found a good fit for HD2 in the extended arm when the α helices are packed roughly perpendicular to this feature (Figures 3A and 3B). In addition, the trajectory of the final α helix (α32) appears to be different in the apoptosome, as we identified a spur of this size that extends from the base of the arm near the regulatory region. This spur was modeled by a simple rotation of α32 about its linker with α31 (Figures 3B and 3E). We then docked the WHD into the map by using its shape and connectivity constraints with HD2 (Figures 3A and 3B). At this stage, there was room for the nucleotide binding domain adjacent to the WHD, and the NBD was docked accurately in this region by using its shape (Figure 3A). In the final step, HD1 was docked into a protrusion on the central hub, and the last α helix in this domain (α19) forms a ridge on the surface (Figure 3C). Hence, our modeling shows that seven HD1s form the crown-like feature on the central hub. In addition, α helix 19 makes a connection to the WHD that involves the L2 linker. This long connection includes α helix 20 in the WHD, which is not in density and may be flexible. Finally, the distance between HD1 and the NBD in our model is consistent with the length of the linker between them.

The Regulatory Region and Cytochrome c

The regulatory region in Apaf-1 is comprised of 13 WD40 repeats, which follow helical domain 2 (Figure 2A). The WD40 repeats are clustered in groups of seven and six in the sequence and form two β propellers with seven and six blades within the regulatory region (Acehan et al., 2002). These features are more clearly defined in the new map. In particular, the map confirms that the β propellers are packed nearly perpendicular to each other, with the smaller β propeller being closer to the central hub (Figure 1D). Since we do not have atomic structures for the Apaf-1 β propellers, our initial assignments were reevaluated with domains from transducin Gβ and TolB, respectively. In this analysis, we found that the seven-bladed β propeller from transducin Gβ fits well within the density for this feature (Figures 3D–3F). In addition, the six-bladed β propeller from TolB is also an excellent fit, as the pseudo-6 fold rotational symmetry is clearly represented in the map (Figure 3E). Both disk-like β propellers have a flat side, a puckered opposing surface, and a central pore that could be fit within the map. However, we could not ascertain the precise

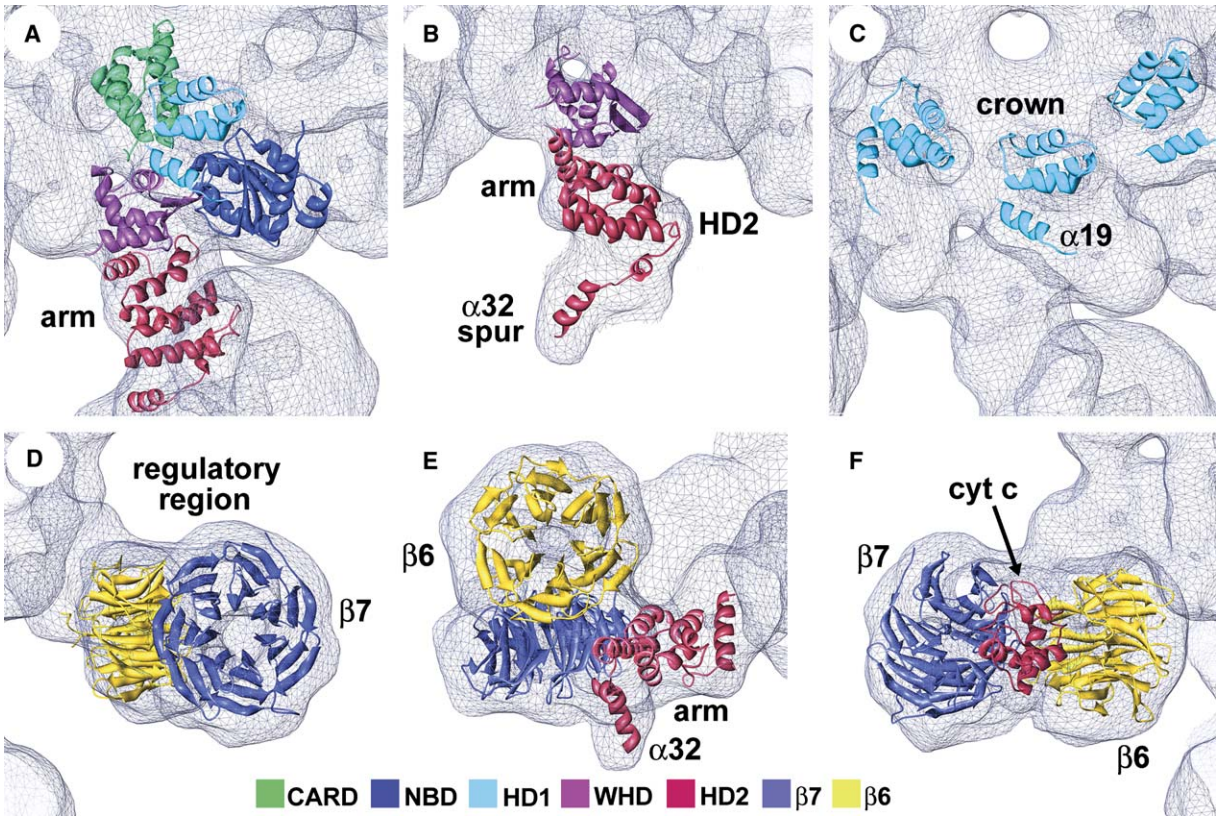

Figure 3. Domains within the Hub, Arm, and Regulatory Region of the Apoptosome

(A) The HD2 arm, WHD, NBD, HD1, and CARD within a single Apaf-1 subunit are shown as ribbons, while the 3D map is viewed as a meshwork. This is an oblique view from the top. Domains have been color coded as indicated (bottom).

(B) HD2 and the WHD fit well within the arm and central hub, respectively. The last α helix in HD2 (α32) was reoriented to fit into the spur.

(C) Seven HD1s create a crown on the central hub. Only three domains are shown in this oblique top view. The last α helix in HD1 (α19) fits within a ridge of density on the top surface of the hub.

(D) The seven-bladed β propeller from transducin Gβ is shown within the regulatory region in a face-on view. The six-bladed β propeller from TolB is seen from the side in this view.

(E) A face-on view of the six-bladed β propeller from TolB is shown within the regulatory region. The seven-bladed β propeller and HD2 arm are also shown.

(F) Cytochrome c fits snugly into a V-shaped slot between the two β propellers.

rotational alignment of the β propellers due to their pseudosymmetry. This uncertainty dissuaded us from creating homology models for the β propellers to use in the docking.

Cytochrome c has a remarkable dual life as an electron carrier in the mitochondrial respiratory chain and as a trigger for apoptosome assembly (Liu et al., 1996; Li et al., 1997; Hao et al., 2005). We previously identified a feature between the two β propellers as cytochrome c (Acehan et al., 2002). We now confirm this assignment, as the new map allowed us to unambiguously dock a single cytochrome c between the β propellers. In this docking, the longer axis of cytochrome c is aligned parallel to the opposing faces of the disk-like WD40 domains (Figure 3F). The cytochrome c density is quite strong, which indicates a high occupancy in the binding site. Hence, the regulatory region in the human apoptosome is comprised of two β propellers with a single cytochrome c slotted in between them. After accounting for all of the electron density in the 3D map, we conclude that the stoichiometry of cytochrome c to Apaf-1 in the recombinant apoptosome is 1:1 rather than 2:1 (Purring et al., 1999).

A Domain Model of the Apoptosome

Our model of the apoptosome provides appropriate connectivity between domains with short linkers (NBD-HD1, WHD-HD2) and provides a good overall fit for domains within the 3D density map. The model also confirms many details of the wheel-like apoptosome (Acehan et al., 2002), but it places them in sharper focus. We find that Apaf-1 starts near the center of the apoptosome, runs through the central hub, and extends into the regulatory region. However, a more detailed analysis is now possible. Thus, the N-terminal CARDs from seven Apaf-1 subunits converge to form a central CARD ring that represents the active center of the apoptosome (Figures 4A–4D, see green ring). In support of this assignment, procaspase-9 was shown to bind to this region of the apoptosome (Acehan et al., 2002). The finding that seven CARDs form a discrete ring suggests that they may function as a cooperative unit in the apoptosome. Each CARD also makes contacts with the NBD through the L1 linker (Riedl et al., 2005). In addition, a crown of seven HD1s sits atop the CARD ring (Figures 4A and 4C) and may partially block access of procaspase-9 to the CARDs. During assembly, adjacent

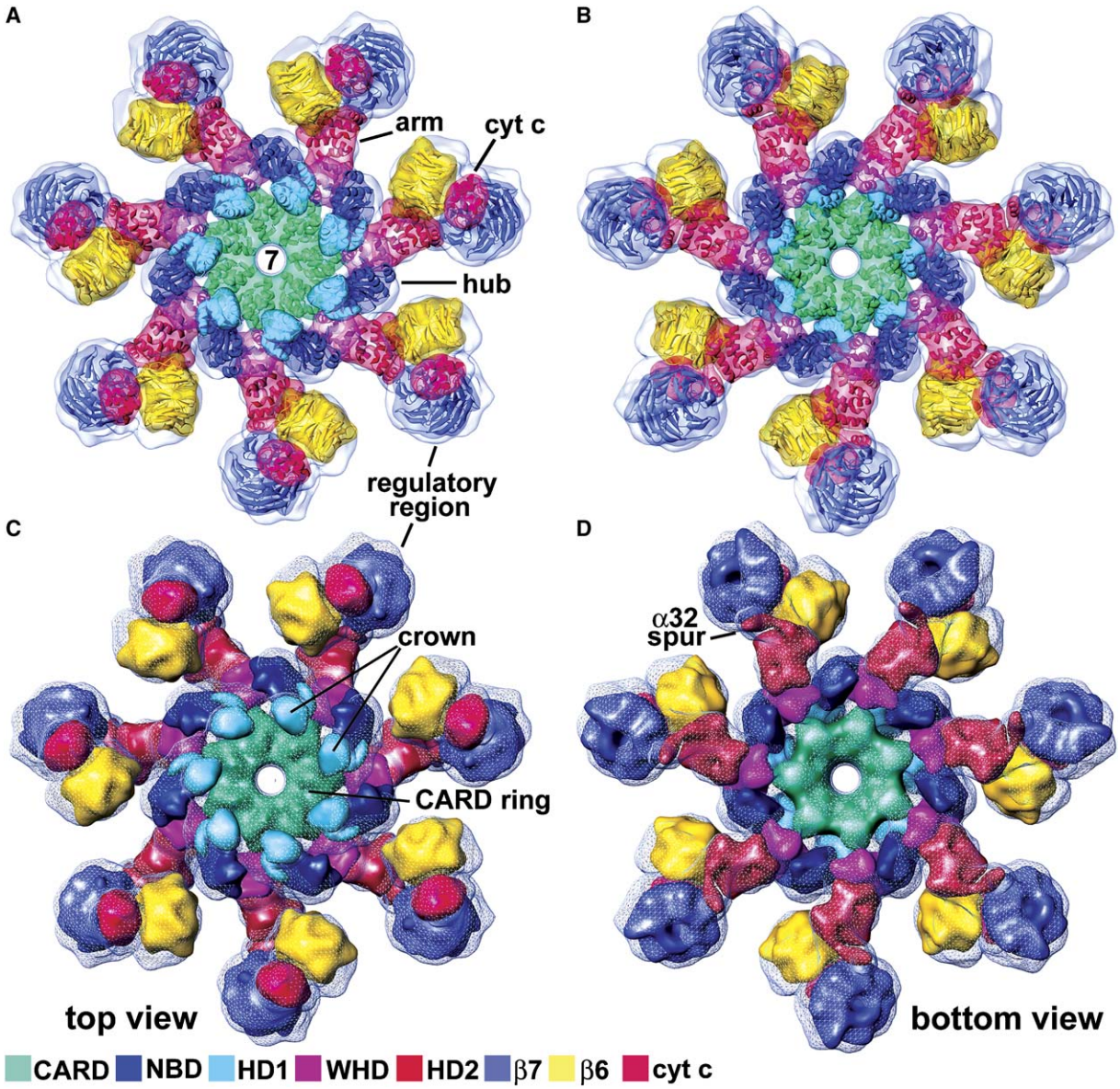

Figure 4. Domain Architecture of the Human Apoptosome

(A) A top view of the human apoptosome is shown with the 3D map rendered as a transparent surface. Individual domains are shown as ribbons within a transparent molecular surface that was calculated for each domain at 12 Å resolution. Domains are color coded as indicated (bottom), and major features of the apoptosome are labeled. Small gaps between the CARD ring and the central hub are present because the L1 linker was not modeled. The figure was made with Chimera and SPIDER.

(B) A bottom view of the apoptosome is shown with graphics like those used in (A). Contributions to the central hub of the WHD, NBD, and HD2 are readily apparent.

(C) A top view of the apoptosome is shown with the 3D map rendered as a meshwork. Individual domains are shown as color-coded solid surfaces at 12 Å resolution, to give a space filling view of the domain model. The CARD ring and the HD1 crown are labeled. Cytochrome c fits snugly between the two β propellers in the regulatory region.

(D) A bottom view of the apoptosome is shown with graphics like those used in (C). Alternating interactions in the central hub between adjacent NBD and winged helix domains are apparent. The α32 spur is labeled and extends toward the reader in this view.

Apaf-1 subunits pack together in a cylindrical manner to form the central hub, which encircles the CARD ring. The hub is stabilized by interactions between the nucleotide binding domain in one subunit and a winged helix domain in an adjacent subunit, but the N-terminal region of HD2 (the proximal surface of the arm) also contributes. This can be observed clearly in top and bottom views of the apoptosome (Figures 4A–4D).

The apoptosome contains bound dATP when the complex is assembled with this nucleotide (Jiang and Wang, 2000). In addition, a nonhydrolyzable ATP analog (AMP-PCP) can substitute for dATP during assembly of a functional apoptosome (Jiang and Wang, 2000). Since we used a large excess of dATP (0.1 mM) during assembly and Apaf-1 is a poor dATPase (Jiang and Wang, 2000), we wondered if Apaf-1 would be in a dATP-like

conformation in our 3D model. To test this hypothesis, we assembled apoptosomes in AMP-PCP with conditions that were similar to those used to prepare the EM samples. As shown in Figure 1A, apoptosomes made with AMP-PCP (right, labeled AMP-PCP) or dATP (left, standard assembly) had similar mobilities on glycerol gradients, and both complexes contained cytochrome c. When taken together, the data suggest that Apaf-1 domains that bind nucleotide (NBD and HD1) may be in a dATP-like conformation in our map. Indeed, the relative orientations of the NBD and HD1 differ significantly in the apoptosome when compared to their positions in the crystal structure of Apaf1-591 with a bound ADP (Riedl et al., 2005; see Discussion).

A second helical domain (HD2) forms the arm of Apaf-1 and extends outward from the central hub. This domain also makes distal interactions with the regulatory region. Intriguingly, HD2 uses "pairs" of α helices to form the arm, a feature that is reminiscent of α-helical pairs in clathrin arms (Fotin et al., 2004), but this motif occurs on a smaller scale in Apaf-1. Finally, the C-terminal regulatory region is formed by a pair of β propellers that contain seven and six blades. These β propellers form a V-shaped binding site for a single molecule of cytochrome c.

Our model also highlights the role of two linkers. The L1 link between the CARD and NBD may facilitate conformational changes that release the CARD from the NBD, upon activation by cytochrome c. Intriguingly, an Apaf-1 isoform was initially identified that contained a shorter L1 linker (~9 residues) and 12 WD40 repeats (see Hu et al., 1999; Zou et al., 1999), but it is not known whether the short linker is responsible for the low activity of this molecule. While the L2 linker between HD1 and the WHD is not in density at the current resolution, it plays an important role in positioning these domains in the central hub.

Forming Rings with the Nucleotide Binding Domain

This domain model of the apoptosome helps to explain the pivotal roles of the NBD, HD1, and winged helix domains, as they form the central hub and constitute a functional NOD. Thus, the apoptosome may provide a paradigm for the formation of ring-like oligomers by NOD family members from bacteria, plants, and animals (Leipe et al., 2004; Inohara and Nunez, 2003). In addition, a similar NBD and associated small helix domain (HD1-like) is generally conserved in the P loop NTPase superfamily, which includes the AAA+ ATPases (Leipe et al., 2004, Riedl et al., 2005). Remarkably, the NBD and HD1 are used quite differently in the Apaf-1 heptamer when compared to the NSF D2 and p97 D1 hexamers (Yu et al., 1998; Zhang et al., 2000). In the apoptosome, alternating contacts between the NBD and WHD help form the central hub and create a large central cavity that contains the CARD ring, while HD1 forms a crown on the top surface (Figure 5A). In contrast, the NBD of NSF makes contacts with neighboring NBDs to form the D2 hexameric ring (Figure 5B; Yu et al., 1998). In the NSF hexamer, ATP is bound between the NBD and the small HD1-like region. At present, the role of the winged helix-like domain in the AAA+ ATPases remains unclear. We surmise that at least two different mechanisms have evolved within the P loop NTPase superfamily to create ring-like oligomers. In addition, many NOD family members have N-terminal effector domains that are not CARDs. Our data suggest that domains of the central hub (along with the N-terminal region of the HD2 arm) may be sufficient to promote ring formation by these NOD proteins.

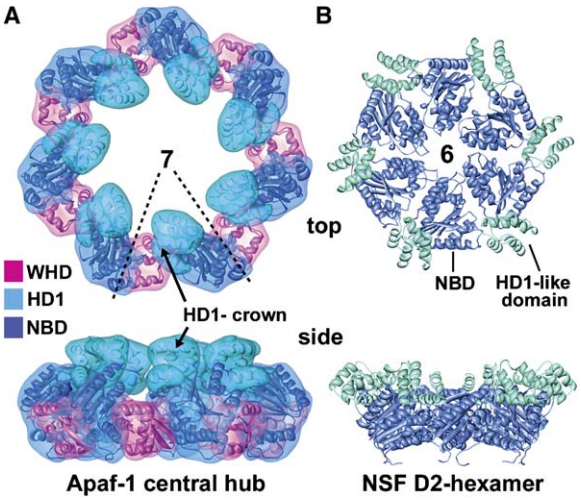

Figure 5. Ring-like Oligomers of Apaf-1 and NSF-D2 Assemble in Different Ways

(A) The NBD and WHD combine to form a heptameric hub with a large central cavity (top). This space is filled by the CARD ring in the apoptosome. Seven HD1s form a crown that sits on top of the central hub (see top and side views). The NBD, HD1, and WHD in a single Apaf-1 subunit are delineated by a dashed line.

(B) The conserved NSF NBD interacts with NBDs in adjacent subunits to form a tightly packed hexameric ring in the D2 hexamer (top, 1NSF). A small α-helical domain follows the NBD and is homologous to HD1 (in cyan). This small α-helical domain helps to bind nucleotide and sits "on top" of the D2 ring (side view). A single subunit is labeled, and ATP is bound in the interface between the NBD and HD1-like domain.

Discussion

In this work, we have determined a structure of the human apoptosome at 12.8 Å resolution. We then used molecular docking with known crystal structures to create an accurate domain model for Apaf-1 within the apoptosome. Thus, our model reveals a CARD ring at the center of the apoptosome and provides a detailed snapshot of this large death platform. When combined with biochemical data, the improved model provides a rationale for the roles of cytochrome c and dATP in assembly. Finally, our model reveals how the CARD ring and hub create an activation platform for procaspase-9.

Assembly of the Apoptosome

In the mitochondrial pathway, Apaf-1 assembles into an apoptosome that plays a central role in the activation of procaspase-9 (Li et al., 1997; reviewed in Danial and Korsmeyer, 2004; Green and Evan, 2002). This pathway is particularly important in the development of the central nervous system (Ferraro et al., 2003) and is also used for apoptosis induced by radiation and chemotherapeutic agents. Thus, it is clearly important to understand apoptosome assembly, and recent data allow us to suggest a working hypothesis for this event.

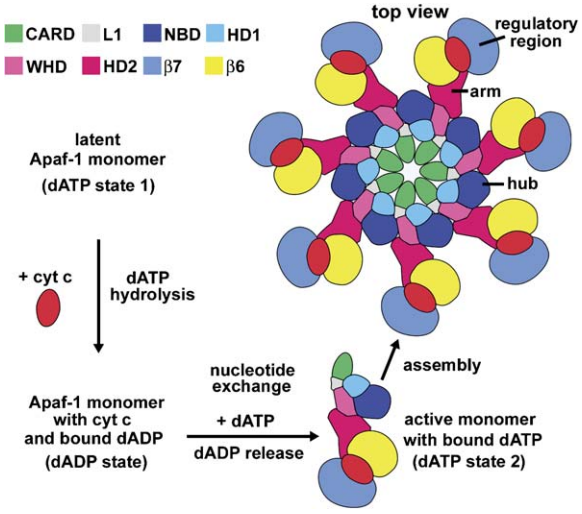

Figure 6. An Assembly Model for the Human Apoptosome

(Upper left) The latent form of Apaf-1 may form a compact monomer (Acehan et al., 2002), presumably with the regulatory region chaperoning the NOD, which contains a bound dATP. (Lower left) Cytochrome c binds to the regulatory region to trigger one cycle of dATP hydrolysis by Apaf-1, and this creates a dADP bound conformation of the monomer. (Lower right) Nucleotide exchange (dATP for dADP) and interactions with other Apaf-1 monomers or with procaspase-9 may lead to an extended conformation that assembles into the apoptosome. (Upper right) Apoptosome assembly may be driven by lateral interactions between the NBD and WHD in adjacent subunits. This assembly process may allow the CARDs to form a central ring that represents the active center of this death platform.

Cytochrome c is required for apoptosome assembly (Liu et al., 1996; Li et al., 1997). Thus, pro-death members of the Bcl-2 family play a role in permeabilizing the outer mitochondrial membrane, which sets the stage for cytochrome c release into the cytosol, where it binds Apaf-1 with high affinity (see Newmeyer and Ferguson-Miller, 2003). Our maps show that one cytochrome c molecule is bound between two β propellers in the regulatory region of Apaf-1 (Acehan et al., 2002 and this study). Cytochrome c binding may release the NOD of Apaf-1 from the WD40 domains, thereby creating a more extended molecule (Figure 6; Acehan et al., 2002). The binding of cytochrome c may also have direct ramifications for the dATPase cycle of Apaf-1 (see below).

Previous studies have shown that dATP is bound to the apoptosome when this nucleotide is used for assembly (Jiang and Wang, 2000). In addition, the measured rate of dATP hydrolysis by purified Apaf-1 is very low (~1 dATP/Apaf-1/hr) and is similar in the presence of cytochrome c and procaspase-9 (Jiang and Wang, 2000). In addition, a structure-based alignment (Riedl et al., 2005) shows that two aspartate residues in the Walker B box of Apaf-1 are replaced by Leu-Asn in Dark, the *Drosophila* homolog of Apaf-1. These acidic residues mediate interactions with Mg^{2+} and a nucleophilic water and are critical to NTPase activity. Hence, both Apaf-1 and Dark appear to be rather poor dATPases.

When taken together, these observations present a conundrum, since additional dATP is required for apoptosome assembly in cell extracts and with purified Apaf-1. However, recent observations suggest that dATP bound to the latent Apaf-1 monomer may be hydrolyzed during the binding of cytochrome c (Kim et al., 2005). Hence, nucleotide hydrolysis may create an Apaf-1 monomer with a bound dADP that represents an assembly intermediate. In this process, cytochrome c would function like a dATPase activation protein (a dAAP) for one cycle of dATP hydrolysis by Apaf-1 (Figure 6, left). In addition, dATP binding to purified Apaf-1 is increased ~20-fold in the presence of cytochrome c and procaspase-9 (Jiang and Wang, 2000; Liu et al., 1996; Li et al., 1997), which is presumably due to hydrolysis of bound dATP. The addition of dATP after cytochrome c binding may facilitate nucleotide exchange on Apaf-1 (Figure 6, bottom) and create a second dATP bound conformation that is amenable to assembly. Indeed, dATP can be replaced in this step with a nonhydrolyzable ATP analog without affecting assembly (AMP-PCP; Jiang and Wang, 2000; this work). Thus, Apaf-1 may have two distinct dATP binding conformations: one that stabilizes the latent monomer (dATP state 1) and one that leads to assembly (dATP state 2). Moreover, a defined dADP-like conformation of Apaf-1 must exist between the two dATP states.

In any case, once an open conformation of Apaf-1 with bound dATP is attained, it may coassemble with six other subunits to form the apoptosome. In this step, the NBD and WHD in the Apaf-1 subunits may associate in a cylindrical manner to form the central hub, and the CARDs may assemble the CARD ring (Figure 6, right). However, it is worth noting that the isolated Apaf-1 CARD exists as a monomer in solution (Qin et al., 1999; Zou et al., 1999); hence, the lateral association of multiple CARDs may, by itself, be insufficient to promote apoptosome assembly. Alternatively, assembly may be favored by procaspase-9 binding to the CARD, since the Apaf-1 CARD oligomerizes in the presence of procaspase-9 (Shiozaki et al., 2002).

Given this assembly model, we may ask: Where might the ADP bound conformation of Apaf1-591 be positioned within the proposed pathway? A comparison of the relative orientation of HD2 and the WHD shows that they are similar in the crystal structures of Apaf1-591 and the apoptosome (Figure 7A). Hence, the regulatory region of Apaf-1 may fit onto the HD2 arm of Apaf1-591 without a major perturbation. Since the nucleotide in the crystal structure is ADP, we suggest that the domain organization of Apaf1-591 may approximate the dADP assembly intermediate in Figure 6 (lower left). Of course many questions remain. In particular, it is apparent that the enclosed dADP/ADP must be exchanged for a nucleotide triphosphate in order for assembly to proceed. We predict that nucleotide exchange will be accompanied by major rearrangements of the CARD, NBD, and HD1 in going from a dADP state to the second dATP state (arrows in Figure 7A). This exchange (dATP for dADP) may be facilitated by breathing motions of the domains or by procaspase-9 binding and interactions with other Apaf-1 monomers (Jiang and Wang, 2000).

An Activation Platform for Procaspase-9

In our model, we oriented the Apaf-1 CARDs such that their procaspase-9 binding surfaces are exposed on the top of the CARD ring. Hence, the CARD ring creates a dense-packed, radial array of binding sites for the

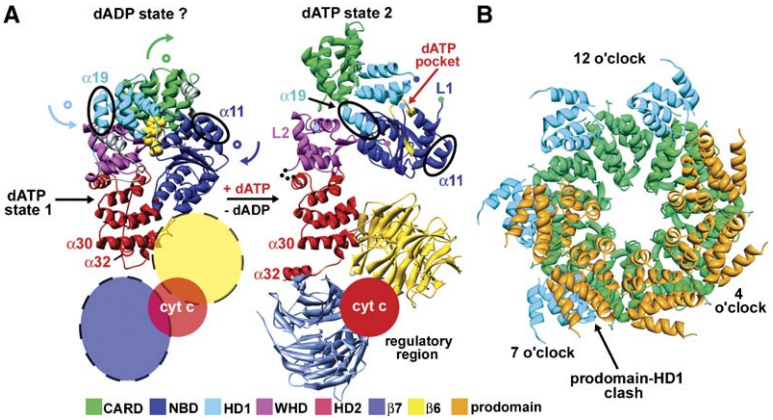

Figure 7. Apaf-1 Conformations during Assembly and Procaspase-9 Binding to the CARD Ring

(A) A self-inhibited Apaf-1 monomer with bound dATP (dATP state 1) may hydrolyze dATP upon binding cytochrome c. This would create an Apaf-1 conformation with bound dADP (dADP state) that may be similar to the Apaf1-591 structure (Riedl et al., 2005). Approximate positions of the β propellers and cytochrome c are indicated in this hypothetical intermediate. Nucleotide exchange and the formation of an assembly-competent Apaf-1 monomer (dATP state 2) may require a reorientation of the CARD, NBD, and HD1 as shown (see arrows in dADP state).

(B) The HD1 crown is shown in cyan between 11 and 1 o'clock, as modeled in the unliganded apoptosome. The HD1 crown blocks access of the procaspase-9 prodomain (shown in orange) to the central CARD ring, as shown by a strong clash between these domains in the region from 7 to 9 o'clock. However, when the HD1 crown is removed, multiple prodomains can dock to adjacent CARDs without a serious clash (2–6 o'clock). Thus, seven HD1s may adopt a different orientation in the central hub of the holo-apoptosome.

prodomain of procaspase-9 (Figure 7B, from 2 to 6 o'clock). However, the HD1 crown (Figure 7B, shown in cyan at 11–1 o'clock) would block prodomain access to these sites when zymogen is added to apoptosomes (Figure 7B, 7–9 o'clock). The situation in vivo is different because procaspase-9 could interact with Apaf-1 during assembly. Thus, Apaf-1/procaspase-9 complexes may form in the presence of cytochrome c and coassemble when dATP is bound, to form an active holo-apoptosome. In both cases, HD1 may be positioned differently to minimize a clash with procaspase-9 in the holo-apoptosome. In line with this idea, we have observed a large upward movement of the top surface of the central hub when procaspase-9 is bound to the apoptosome (Acehan et al., 2002).

Finally, the close proximity of 7 procaspase-9 binding sites on the CARD ring may be compensated to some extent by the presence of a long (45 residues) linker between the prodomain and large subunit of this zymogen. Given this binding geometry, a simple calculation suggests that the local concentration of procaspase-9 may approach ~200 mg/ml on the hub, when all seven CARDs are saturated with zymogens. Indeed, there appears to be no reason why seven procaspase-9 monomers could not bind simultaneously to the apoptosome. This high local concentration of zymogen may favor dimer formation by monomer recruitment from solution (Boatright et al., 2003; Acehan et al., 2002; Renatus et al., 2001), or it may favor lateral interactions between procaspase-9 molecules that cannot otherwise occur in solution (Chao et al., 2005, Shi, 2002). Hence, the precise details of procaspase-9 binding and activation on the holo-apoptosome remain to be elucidated.

Experimental Procedures

Apaf-1 Purification and Assembly

Apaf-1 was expressed, purified, and assembled in buffer A (20 mM HEPES-KOH [pH 7.5], 10 mM KCl, 1.5 mM $MgCl_2$, 1 mM EDTA, 1 mM EGTA, 1 mM dithiothreitol) with cytochrome c (Apaf-1 to cytochrome c molar ratio = 1:1.5) and 0.1 mM dATP (Acehan et al., 2002). However, the apoptosomes were concentrated to 5–8 mg/ml by using a Microcon YM-30 (from Millipore), in the presence of Nonidet P40 (final concentration of ~0.1%–0.2%). To monitor assembly, apoptosomes were run on a 10%–40% glycerol gradient (volume = 2.2 ml) in buffer A at 17ºC for 2.5 hr in an RP55S rotor (55,000 rpm; Sorval). Fractions were collected manually from the top in ~150 μl aliquots, separated by SDS-PAGE on an 8%–15% gradient gel, and visualized with Coomassie blue. For the salt stability test, apoptosomes were assembled in buffer A supplemented to a final salt concentration of 100 mM KCl. After assembly, the complexes were concentrated and run on a glycerol gradient in the same buffer. To test assembly with a nonhydrolyzable analog, AMP-PCP at 0.1 mM (Sigma-Aldrich) was used instead of dATP.

Electron Cryomicroscopy, Structure Determination, and Modeling

Two independent 3D data sets were collected from frozen-hydrated particles. To prepare specimens for the map at 21 Å resolution, holey Quantifoil grids (400 mesh) were coated with carbon, and the film was rendered hydrophobic by incubation in an oven at ~70ºC for ~1 hr. Aliquots (2 μl) of the concentrated sample were pipetted onto the grids, which were subsequently blotted and plunge frozen in liquid ethane in a humid chamber at 4ºC (Acehan et al., 2002). Electron micrographs were collected on Kodak film with a JEOL 2010SFF microscope at the National Center for Macromolecular Imaging. Images were collected at 200 kV and a nominal magnification of 50,000×. For the final map, data were collected on film at 50,000× with a Tecnai F20 microscope. In these experiments, plastic films with a random distribution of small holes (Fukami and Adachi, 1965) were floated and picked up on 300 or 400 mesh Cu grids. After carbon shadowing, the plastic was removed from the grids with ethyl acetate, and the carbon film was glow discharged in an air-isopropanol mixture. Frozen-hydrated specimens were then prepared as described above. This approach produced better specimen contrast because the ice was thinner. In addition, images were taken at 120 kV rather than 200 kV to further enhance specimen contrast.

Electron micrographs were evaluated by optical diffraction for astigmatism and drift. Good negatives were scanned with an Eversmart scanner (Creo, Inc.) with a step size of 4.54 μm and binned to 2.73 Å/pixel. Particles were selected by using BOXER (Ludtke et al., 1999), and a full CTF correction was done by using CTFIT and a hybrid structure factor curve. The low-resolution region of the structure factor was obtained from apoptosome images, and the remainder of the curve was obtained from a published profile of GroEL (Ludtke et al., 2004). For the map at 21 Å, our previously published structure (Acehan et al., 2002) was used as a starting 3D reference. In this analysis, we started with ~10,000 particles, and ~5,400 were used in the final reconstruction. For the final 3D map, the model at 21 Å resolution (Figure S1, middle) was used as the initial reference. About 13,000 particles were used to start this refinement, and ~7,600 were included in the final reconstruction. The setsf option was used during the final refinement steps with a classkeep of 0.2. The resolution was estimated from the Fourier Shell Correlation (FSC) in EMAN by using a cutoff of 0.5.

An initial docking with the relevant domains was carried out manually in O (Jones, et al., 1991), by using overall fit and connectivity within a subunit of the apoptosome. At this stage, we identified the correct hand of the map based on the best global fit. For this work, the first five domains of Apaf-1 were taken from Apaf1-591 (1Z6T; Riedl, et al., 2005). Models for the seven-bladed β propeller (1GFW), the six-bladed β propeller (1CRZ), and cytochrome c (3CYT) were also used. After the initial docking, related subunits were generated by using a 7-fold symmetry matrix in Moleman2 (Kleywegt et al., 2004). Domains in the model were subsequently refined as rigid bodies by using RSRef2000 to maximize the cross-correlation value between the model and the map (Fabiola and Chapman, 2005), and, in some cases, the domains were adjusted manually. The final crosscorrelation coefficient (0.67) indicates the overall fit of the model at this resolution, but it also reflects the fact that the β propellers, which account for ~50% of the molecule, are not from Apaf-1. Figures were made with Web (Frank et al., 1996), Chimera (Goddard et al., 2005), and Adobe Photoshop.

Supplemental Data

Supplemental Data including two figures are available at http://www.structure.org/cgi/content/full/13/11/1725/DC1/.

Acknowledgments

We thank the Scientific Computing and Visualization Group at Boston University for use of a Linux cluster. We also thank Fenghe Du for preparing human Apaf-1 and Preethi Chandramouli for helpful discussions concerning the docking. Coordinates for the apoptosome domain model are available upon request. The S.J.L., Y.S., X.W., and C.W.A. laboratories are supported by National Institutes of Health grants. X.W. was also supported by the Welch Foundation.

Received: August 12, 2005
Revised: September 22, 2005
Accepted: September 26, 2005
Published: November 8, 2005

References

Acehan, D., Jiang, X., Morgan, D.G., Heuser, J.E., Wang, X., and Akey, C.W. (2002). Three-dimensional structure of the apoptosome: implications for assembly, procaspase-9 binding and activation. Mol. Cell *9*, 423–432.

Boatright, K.M., Renatus, M., Scott, F.L., Sperandio, S., Shin, H., Pedersen, I.M., Ricci, J.E., Edris, W.A., Sutherlin, D.P., Green, D.R., and Salvesen, G.S. (2003). A unified model for apical caspase activation. Mol. Cell *11*, 529–541.

Budihardjo, I., Oliver, H., Lutter, M., Luo, X., and Wang, X. (1999). Biochemical pathways of Caspase activation during apoptosis. Annu. Rev. Cell Dev. Biol. *15*, 269–290.

Chao, Y., Shiozaki, E.N., Srinivasula, S.M., Rigotti, D.J., Fairman, R., and Shi, Y. (2005). Engineering a dimeric caspase-9: a re-evaluation of the induced proximity model for caspase activation. PLoS Biol. *3*, e183.

Danial, N.N., and Korsmeyer, S.J. (2004). Cell death: critical control points. Cell *116*, 205–219.

Desagher, S., and Martinou, J.-C. (2000). Mitochondria as the central control point of apoptosis. Trends Cell Biol. *10*, 369–377.

Fabiola, F., and Chapman, M.S. (2005). Fitting of high-resolution structures into electron microscopy reconstruction images. Structure *13*, 389–400.

Ferraro, E., Corvaro, M., and Cecconi, F. (2003). Physiological and pathological roles of Apaf1 and the apoptosome. J. Cell. Mol. Med. *7*, 21–34.

Fotin, A., Cheng, Y., Sliz, P., Grigorieff, N., Harrison, S.C., Kirchhausen, T., and Walz, T. (2004). Molecular model for a complete clathrin lattice from electron cryomicroscopy. Nature *432*, 573–579.

Frank, J., Radermacher, M., Penczek, P., Zhu, J., Li, Y., Ladjadj, M., and Leith, A. (1996). SPIDER and WEB: processing and visualization of images in 3D electron microscopy and related fields. J. Struct. Biol. *116*, 190–199.

Fukami, A., and Adachi, K. (1965). A new method of preparation of a self-perforated micro plastic grid and its application. J. Electron Microsc. *14*, 112–118.

Goldstein, J.C., Waterhouse, N.J., Juin, P., Evan, G.I., and Green, D.R. (2000). The coordinate release of cytochrome c during apoptosis is rapid, complete and kinetically invariant. Nat. Cell Biol. *2*, 156–162.

Goddard, T.D., Huang, C.C., and Ferrin, T.E. (2005). Software extensions to UCSF chimera for interactive visualization of large molecular assemblies. Structure *13*, 473–482.

Green, D.R., and Evan, G.I. (2002). A matter of life and death. Cancer Cell *1*, 19–30.

Hao, Z., Duncan, G.S., Chang, C.C., Elia, A., Fang, M., Wakeham, A., Okada, H., Calzascia, T., Jang, Y., You-Ten, A., et al. (2005). Specific ablation of the apoptotic functions of cytochrome c reveals a differential requirement for cytochrome C and Apaf-1 in apoptosis. Cell *121*, 579–591.

Hill, M.M., Adrain, C., Duriez, P.J., Creagh, E.M., and Martin, S.J. (2004). Analysis of the composition, assembly kinetics and activity of native Apaf-1 apoptosomes. EMBO J. *23*, 2134–2145.

Hu, Y., Ding, L., Spencer, D.M., and Nunez, G. (1998). WD-40 repeat region regulates Apaf-1 self-association and procaspase-9 activation. J. Biol. Chem. *273*, 33489–33494.

Hu, Y., Benedict, M.A., Ding, L., and Nunez, G. (1999). Role of cytochrome c and dATP/ATP hydrolysis in Apaf-1 mediated caspase-9 activation and apoptosis. EMBO J. *13*, 3591–3595.

Inohara, N., and Nunez, G. (2003). NODs: intracellular proteins involved in inflammation and apoptosis. Nat. Rev. Immunol. *3*, 371–382.

Jiang, X., and Wang, X. (2000). Cytochrome c promotes caspase-9 activation by inducing nucleotide binding to apaf-1. J. Biol. Chem. *275*, 31199–31203.

Jones, T.A., Zou, J.-Y., and Cowan, S.W. (1991). Improved methods for building protein models in electron density maps and the location of errors in these models. Acta Crystallogr. A *47*, 110–119.

Kim, H.-E., Du, F., Fang, M., and Wang, X. (2005). Formation of an apoptosome is initiated by cytochrome c induced dATP hydrolysis and subsequent nucleotide exchange on Apaf-1. Proc. Natl. Acad. Sci. USA, in press.

Kleywegt, G.J., Harris, M.R., Zou, J.Y., Taylor, T.C., Wahlby, A., and Jones, T.A. (2004). The Uppsala electron-density server. Acta Crystallogr. D Biol. Crystallogr. *60*, 2240–2249.

Kuwana, T., and Newmeyer, D.D. (2003). Bcl-2-family proteins and the role of mitochondria in apoptosis. Curr. Opin. Cell Biol. *15*, 691–699.

Leipe, D.D., Koonin, E.V., and Aravind, L. (2004). STAND, a class of P-loop NTPases including animal and plant regulators of programmed cell death: multiple, complex domain architectures, unusual phyletic patterns, and evolution by horizontal gene transfer. J. Mol. Biol. *343*, 1–28.

Li, P., Nijhawan, D., Budihardjo, I., Srinivasula, S.M., Ahmad, M., Alnemri, E.S., and Wang, X. (1997). Cytochrome c and dATP-dependent formation of Apaf-1/Caspase-9 complex initiates an apoptotic protease cascade. Cell *91*, 479–489.

Liu, X., Kim, C.N., Yang, J., Jemmerson, R., and Wang, X. (1996). Induction of apoptotic program in cell free extracts: requirement for dATP and cytochrome c. Cell *86*, 147–157.

Ludtke, S.J., Baldwin, P.R., and Chiu, W. (1999). EMAN: semiautomated software for high-resolution single-particle reconstructions. J. Struct. Biol. *128*, 82–97.

Ludtke, S.J., Chen, D.H., Song, J.L., Chuang, D.T., and Chiu, W. (2004). Seeing GroEL at 6 Å resolution by single particle electron cryomicroscopy. Structure *12*, 1129–1136.

Newmeyer, D.D., and Ferguson-Miller, S. (2003). Mitochondria: releasing power for life and unleashing the machineries of death. Cell *112*, 481–490.

Purring, C., Zou, H., Wang, X., and McLendon, G. (1999). Stoichiometry, free energy and kinetic aspects of cytochrome c:Apaf-1 binding in apoptosis. J. Am. Chem. Soc. *121*, 7435–7436.

Qin, H., Srinivasula, S.M., Wu, G., Fernandes-Alnemri, T., Alnemri, E.S., and Shi, Y. (1999). Structural basis of procaspase-9 recruitment by the apoptotic protease-activating factor 1. Nature *399*, 549–557.

Renatus, M., Stennicke, H.R., Scott, F.L., Liddington, R.C., and Salvesen, G.S. (2001). Dimer formation drives the activation of the cell death protease caspase-9. Proc. Natl. Acad. Sci. USA *98*, 14250–14255.

Riedl, S.J., Li, W., Chao, Y., Schwarzenbacher, R., and Shi, Y. (2005). Structure of the apoptotic protease-activating factor 1 bound to ADP. Nature *434*, 926–933.

Rodriguez, J., and Lazebnik, Y. (1999). Caspase-9 and Apaf-1 form an active holoenzyme. Genes Dev. *13*, 3179–3184.

Salvesen, G.S., and Dixit, V.M. (1997). Caspases: intracellular signaling by proteolysis. Cell *91*, 443–446.

Shi, Y. (2002). Apoptosome: the cellular engine for the activation of caspase-9. Structure *10*, 285–288.

Shiozaki, E.N., Chai, J., and Shi, Y. (2002). Oligomerization and activation of caspase-9, induced by Apaf-1 CARD. Proc. Natl. Acad. Sci. USA *99*, 4197–4202.

Song, Z., and Steller, H. (1999). Death by design: mechanism and control of apoptosis. Trend. Cell Biol. *12*, 49–52.

Srinivasula, S.M., Ahmad, M., Fernandes-Alnemri, T., and Alnemri, E.S. (1998). Autoactivation of procaspase-9 by Apaf-1 mediated oligomerization. Mol. Cell *1*, 949–957.

Stennicke, H.R., Deveraux, Q.L., Humke, E.W., Reed, J.C., Dixit, V.M., and Salvesen, G.S. (1999). Caspase-9 can be activated without proteolytic processing. J. Biol. Chem. *274*, 8359–8362.

Thompson, C.B. (1995). Apoptosis in the pathogenesis and treatment of disease. Science *267*, 1456–1462.

Wang, X. (2001). The expanding role of mitochondria in apoptosis. Genes Dev. *15*, 2922–2933.

Yu, R.C., Hanson, P.I., Jahn, R., and Brunger, A.T. (1998). Structure of the ATP-dependent oligomerization domain of N-ethylmaleimide sensitive factor complexed with ATP. Nat. Struct. Biol. *5*, 803–811.

Zhang, X., Shaw, A., Bates, P.A., Newman, R.H., Gowen, B., Orlova, E., Gorman, M.A., Kondo, H., Dokurno, P., Lally, J., et al. (2000). Structure of the AAA+ ATPase p97. Mol. Cell *6*, 1473–1484.

Zou, H., Henzel, W.J., Liu, X., Lutschg, A., and Wang, X. (1997). Apaf-1, a human protein homologous to C. elegans CED-4, participates in cytochrome c dependent activation of caspase-3. Cell *90*, 405–413.

Zou, H., Li, Y., Liu, X., and Wang, X. (1999). An Apaf-1 cytochrome c multimeric complex is a functional apoptosome that activates procaspase-9. J. Biol. Chem. *274*, 11549–11556.